Effectiveness of Wheat Straw Biochar in Aqueous Zn Removal: Correlation with Biochar Characteristics and Optimization of Process Parameters

Divyesh R. Vaghela[1] · Ashish Pawar[1] · Deepak Sharma[1]

Abstract

The adsorption performance of biochar was investigated for the removal of Zn from the aqueous solution. Biochar was produced from three different feedstock: groundnut shell, chickpea straw, and wheat straw using a fixed bed pyrolysis reactor at three different pyrolysis temperatures of 500, 550, and 600 °C for 1 h. The biomass and biochar characterization was performed to examine the elementary composition, surface morphology, and functional group. The response surface methodology with a Box–Behnken design was applied to understand the influence of biochar dose, heavy metal concentration, and contact period on the removal efficiency of Zn from an aqueous solution. The influence of biochar dose and contact time had the most remarkable effect on Zn adsorption. As biochar dose increased from 1 to 3 g/L and contact time from 60 to 180 min, the Zn removal efficiency was found correspondingly increased from 26 to 97%, respectively. The optimum conditions found for the maximum Zn removal are 2.90 g/L biochar dosage, 22 ppm heavy metal concentration, and 309 min contact period were the key parameters to achieve maximum Zn removal efficiency for wheat straw biochar to be around 97.16%. The present experimental investigation concluded that biochar derived from lignocellulosic biomass creates a new window for the appropriate utilization of environmentally friendly adsorbent in wastewater treatment.

Keywords Biochar · Heavy metal · Groundnut shell · Chickpea straw · Adsorption mechanism · Box-Behnken design · Optimization · Response surface methodology

Introduction

Heavy metals are considered toxic pollutants, which creates a hazardous effect on the environment, especially on living organisms, animals, and plant. The important resources responsible for heavy metals (such as Zn, Ng, Cd, Cr, Cu, and Pb) accumulation in aquatic bodies are industrial effluents, human activities, marine waste, untreated sanitary waste [1]. Notably, heavy metals contaminate wastewater also adversely affects human health and causes bacterial, viral, and parasitic diseases [2, 3]. Due to rapid growth in population, commercialization, and civilization, the need for clean water for daily application is increasing in developing countries like India. Therefore, there is an urgent need to safeguard the water resources by purifying and recycling the wastewater. Among the different wastewater treatments, adsorption is recognized as a reliable, cost-effective, and efficient universal method that offers remarkable benefits like its availability, ease of operation, environmentally friendly, effectiveness, and profitability [4].

As a reliable adsorbent, biochar is an organic carbon-rich product of thermal decomposition of biomass in a temperature range between 350 and 700 °C in the absence of air [5]. The physicochemical characteristics of biochar, such as larger surface area, high degree of porosity, availability of oxygen rich functional groups, cation exchange capacity, make it a reliable adsorbent for wastewater treatment. Due to the presence of oxygenated functional groups on the biochar surface occupies a negative charge, therefore adsorbing the positively charged heavy metals or pollutants from wastewater [6]. Therefore, it can be appropriately used as an adsorbent material for lowering the concentration of heavy metals in water bodies. In India, approximately 686 MT of

✉ Ashish Pawar
pawarashishraje123@gmail.com

1 Department of Renewable Energy Engineering, College of Technology and Engineering, Maharana Pratap University of Agriculture and Technology, Udaipur, Rajasthan 313001, India

crop residue is generated annually, out of which 234 MT is available as surplus crop residue, which remains unutilized [7]. So, some peasants in India are burning this surplus crop residue openly, which causes serious environmental issues, especially air pollution. The most widely available crops in the country for agricultural residue generation are cereal crops, oilseed crops, and some cash crops. Among the different crop residues, wheat straw, groundnut shell, and chickpea straw are the primary agricultural residues available in the southern state of India. Country shares around 13.2% of total wheat production, where wheat straw is a by-product and ranks second in production after China. India covers the entire land for wheat crop cultivation is to be around 30.5 million hectares [8]. Similarly, the groundnut shell is one of the popular biomass feedstock due to its low density available in India. Groundnut shell is the byproduct of peanut, having a weight of about 25–30% of the raw peanut [9]. Chickpea straw is residue from the chickpea crop, one of the major pulse crops grown in India. India is one of the largest chickpeas or also known as the bengal gram producing country, and contributes more than 75% of the total world chickpea production [10]. Therefore, management of surplus crop residue and production of biochar for the removal of heavy metals from wastewater has opened a new window in front of the farming and research community. Biochar has enormous potential to manage the effluents through animals or plants, thus reducing its environmental emission load [11]. Many studies are available on biochar production through muffle furnaces and its application in wastewater treatment; however, the increased contact between syngases and produced biochar in muffle furnaces possess a lower surface area and morphological characteristics of biochar [12]. Therefore, in the present experimental investigation, biochar is produced using a pilot-scale fixed bed pyrolysis reactor and evaluated its performance for removal of Zn.

Traditionally, experimental optimization was carried out by investigating the effects on an experimental response of one variable at a time. It was unable to show the interactive effects between the variables studied. It also has a limitation that a series of experiments are needed in one-factor optimization, resulting in a time-consuming and costly process [13]. By optimizing all the critical variables together, the statistical experimental design, such as response surface methodology (RSM), effectively removed the constraints of the conventional method [13, 14]. RSM is one of the promising statistical techniques mainly used to assess the impact of several parameters simultaneously by delivering the more specific condition for a desirable response.

Among the heavy metal concerns, Zn metal is commonly identified in effluent from different sources such as mining, pesticide industries, tanneries, and fertilizer industries. Also, Zn is often more commonly detected in water bodies like rivers, wells, and lakes through different nonpoint sources such

as livestock farms and irrigation fields. Zn metal adversely affects living organisms due to their persistency, toxicity, and bio-accumulation. For example, Zn poisoning in the human body causes dehydration, stomachache, dizziness, electrolyte imbalance, and nausea.

Therefore, keeping the above points in mind, it was decided to use biochar as an adsorbent material for sorption of Zn, which was produced from three different agricultural residues groundnut shell, wheat straw, and chickpea straw for different operating conditions using pilot-scale fixed-bed pyrolysis reactor. The thermal performance of the system was also carried out. The obtained biochar samples were characterized using different analytical techniques such as elementary analyses, fourier transform infrared spectroscopy (FTIR), and scanning electron microscopy (SEM) analyzer. Good quality biochar was used for the adsorption of Zn from wastewater. In the present study, the Zn sorption performance was demonstrated using response surface methodology (RSM) by optimizing different parameters such as biochar dose, heavy metal concentration, and contact time. In addition, a mathematical model was also developed under optimized conditions to understand the systems response.

Material and Methods

Biomass

Groundnut shell, wheat straw, and chickpea straw were collected from the instructional farm of the College of Technology and Engineering, Udaipur, India. Which is located at 24° 35′ 7″ N–latitude, 73° 42′ 45″ E–longitude, and 582.5 m above average sea level. The selected feedstock was cleaned, and particle size was classified into different ranges of particle size, ranging from 10 to 20 mm, followed by solar drying for the removal of excess moisture. The biomass feedstocks were placed in three different airtight containers to restrict the absorption of atmospheric humidity.

Reagent

Zinc nitrate hexahydrate, $Zn(NO_3)_2.6(H_2O)$ was purchased from chemical industry of Udaipur (India). Stock solution of Zn (1000 mg/L) was prepared by dissolving $Zn(NO_3)_2.6(H_2O)$ in deionized water.

Biochar Production

Biochar produced at higher pyrolysis temperature (≥ 500 °C) showed exceptional physicochemical composition in terms of morphology, surface area, presence of functional groups [15, 16]. According to Kim et al. [17], biochar produced at higher temperatures is considered a reliable adsorbent

material for the sorption process. Therefore, in the present study biochar was produced at 500, 550, and 600 °C by keeping 40–60 min of residence time using groundnut shell, wheat straw, and chickpea straw as a feedstock in a pilot-scale fixed bed reactor. A fixed bed pyrolysis reactor is a batch-type system mainly composed of a cylindrically shaped pyrolysis chamber, loading and unloading mechanism, shell, and tube type condenser, heating mechanism, and control panel. The cylindrical pyrolysis chamber made of SS 310 has an inner and outer diameter of 0.36 m and 0.46 m respectively, and the height of the chamber was 0.55 m with a biomass handling capacity to be around 3–4 kg/h. The electrical coils were rolled over the pyrolysis chamber having a 10-kW capacity to achieve desired pyrolysis temperature inside the chamber. The pyrolysis chamber was insulated using a cerawool blanket having a thickness of 5 mm to minimize the heat losses. In the present study, K-type thermocouples were placed at different positions to access the reactor temperature. The temperature controller unit was also coupled with the system to maintain the desired process temperature during the experiment. Groundnut shell, wheat straw, and chickpea straw were fed in the pyrolysis chamber and maintained anaerobic condition by using a mounted lid cover. After reaching the desired temperature inside the reactor selected feedstock were pyrolyzed for 40–60 min of residence time. Then the reactor was cooled down for 24 h duration at room temperature. After cooling at ambient temperature biochar was collected from the reactor. The mass yield of produced biochar from groundnut shell (GSB), wheat straw (WSB), and chickpea straw (CSB) were calculated using the following Eq. (1);

$$
\text{MassYield (\%)} = \frac{\text{Total mass of biochar produced (kg)}}{\text{Mass of biomass (kg)}} \times 100
$$
(1)

Characterization of Biomass and Produced Biochar

Elementary analyses (moisture content, volatile matter, ash content, fixed carbon content, carbon, hydrogen, nitrogen, and oxygen content), hydrogen to carbon, oxygen to carbon ratio, and higher heating value of selected biomass feedstocks were calculated as per the standard protocol ASTM D 3175, ASTM D 3172, and ASTM D 3177 as reported by Vyas et al. [18]. The carbon, hydrogen, nitrogen, and oxygen contents in produced biochar were determined by using CHN/S/O elemental analyzer (Perkin Elmer, Series II, 2400). Surface morphology, porous structure, and the availability of surface functional groups on the biomass and its produced biochar surface were determined by using scanning electron microscope (SEM) ZEISS (EVO-18) and fourier transforms infrared spectroscopy (FTIR) SHIMADZU (8400S) analysis respectively.

Experimental Procedure for the Removal of Zn

The desired solution was prepared using 20 ppm concentration of Zn from the stock solution by taking 2 ml of each Zn solution in a 100-ml volumetric flask and then filling up with water up to the mark in a volumetric flask. Similarly, 40 and 60 ppm Zn solutions were prepared for analysis. Then, the Zn solutions were kept in the conical flask for proper mixing. The above experimental process used 1, 2, and 3 g fine biochar doses. The doses of biochar added to the Zn solution were placed in an Erlenmeyer. A mechanical shaker was used to properly mix the biochar and solution at an ambient temperature. After shaking, the sample was collected out of the shaker and held outside to achieve stability. The sample was filtered using Whatman filter paper no. 42. The resulting filtered sample was analyzed in microwave plasma atomic emission spectroscopy (MP AES) equipment for the detection of Zn concentration in the ionic form. The above experiment was carried out, and the values obtained were considered for RSM (response surface methodology). After each experiment, the Zn removal efficiency was determined as follows:

$$
\text{Removal efficiency (\%)} = \left[\frac{(C_i) - (C_f)}{(C_i)} \right] \times 100
$$
(2)

Where
C_i = initial Zn concentration in the ppm
C_f = final Zn concentration in the ppm

Optimization of Process Variables Through Response Surface Methodology (RSM)

Using a three-factor, three-level Box-Behnken experimental method, including response surface modeling and quadratic programming, the optimal condition for optimizing the adsorption of Zn by biochar was evaluated. The effects of the biochar dosage (g/L), metal ions concentration (ppm), and contact time (min) have been analyzed for this research. Each predictor variables was sequentially coded as A, B, and C at three levels: − 1, 0, and 1. The Box-Behnken designs were generated using three central points for three factors and three levels, comprising fifteen trials. The experimental range and levels of independent variables have been presented in Table 1.

Fifteen experiments were performed, as enumerated in Table 2, for obtaining the percentage of aqueous zinc removed as responses for each experiment. The responses for various experimental conditions were connected by a second degree polynomial equation to the coded variables (A, B, and C) as described below.

Table 1 Experimental ranges and levels of independent variables

Variables	Code	Range and levels		
		Low level (−1)	Centre level (0)	High level (+1)
Biochar dose, (g l^{-1})	A	1	2	3
Heavy metal concentration, (ppm)	B	20	40	60
Contact time, (min)	C	120	240	360

$$Y_k = \beta_o + \sum_{i=1}^{n} \beta_i x_i + \sum_{i=1}^{n} \beta_{ii} x_i^2 + \sum_{i=1}^{n-1} \sum_{j=i+1}^{n} \beta_{ij} x_i x_j \qquad (3)$$

wherever Y_k is the constant coefficient of response (i.e. % decrease in Zn), β_i, β_{ii}, and β_{ij} are. Xi and X_j have coded predictor variables associated exponential to A, B, and C. In the present experimental study, Design Expert 10.0.3 version (State-Ease, Minneapolis, MN) software was used for designing the experiments. For statistical analysis of experimental results, the same program was used.

A complete second-order quadratic model was implemented to compare the independent processing parameters. A second-order polynomial factor was calculated by multiple regression analysis using a design expert for each algorithm term. The obtained results of selected models and regression coefficients were well equipped with the observational result. For each result, the statistical significance of the terms in the regression model is tested through a variance analysis (ANOVA). For judging the appropriateness and effectiveness of the quadratic model, ANOVA is significant. The p values are being used to check the validity of the coefficients, which, in turn, are important to understand the pattern of successful interaction between the factors in the analysis. The magnitude of the p value is inversely proportional to the related coefficient, as a p value below 0.05 means that the terms of the model are important. R^2 and Fisher's test determine the appropriateness of the linear regression.

The desired objectives were selected for factor and interaction. The targets can correspond to any factor or effect. The possible objectives are enhancing, minimizing, targeting, and within range (for responses only). From an economics perspective, all the independent variables (A, B, and C) were held in the range while the results viz. The percentage decline in heavy metals has remained maximized.

Results and Discussion

Elementary Analysis of Biomass

The elementary analyses and higher heating value of groundnut shell, chickpea straw, and wheat straw were investigated using different analytical methods and are listed in Table 3. The elementary analysis of the groundnut shell indicated that the feedstock has a more volatile matter of 77.87%, while lower moisture, ash, and fixed carbon content are around 6.78, 4.58, and 10.77%, respectively. A similar observation was also found for the other two agro residues in chickpea straw, available volatile, moisture, ash, and fixed

Table 2 Box–Behnken design matrix with three independent variables expressed in coded and uncoded values

Batch no	Biochar dose, (g l^{-1})		Heavy metal concentration, (ppm)		Contact time, (min)	
	X_1 (coded)	X_1 (uncoded)	X_2 (coded)	X_2 (uncoded)	X_3 (coded)	X_3 (uncoded)
1	−1	1	−1	20	0	240
2	1	3	−1	20	0	240
3	-1	1	1	60	0	240
4	1	3	1	60	0	240
5	−1	1	0	40	−1	120
6	1	3	0	40	−1	120
7	−1	1	0	40	1	360
8	1	3	0	40	1	360
9	0	2	−1	20	−1	120
10	0	2	1	60	-1	120
11	0	2	−1	20	1	360
12	0	2	1	60	1	360
13	0	2	0	40	0	240
14	0	2	0	40	0	240
15	0	2	0	40	0	240

Table 3 Elementary analysis of biomass and biochar

Sr. no	Biomass sample	Moisture content, (%)	Volatile matter, (%)	Ash content, (%)	Fixed carbon, (%)	HHV, (MJ/kg)	Carbon (C), %	Hydrogen (H), %	Nitrogen (N), %	Oxygen (O), %	H/C	O/C
1	Groundnut shell	6.78±0.2	77.87±0.17	4.58±0.01	10.77±0.2	16.23±0.54	50.12±1.17	5.41±0.04	0.6±0.01	42.80±0.55	1.29±0.01	0.64±0.01
2	Chickpea straw	8.71±0.1	68.91±0.15	11.52±0.2	10.86±0.1	15.21±0.23	48.10±1.10	5.23±0.02	0.4±0.01	42.31±0.68	1.30±0.01	0.65±0.01
3	Wheat straw	9.18±0.1	66.12±0.14	7.9±0.02	16.8±0.1	14.74±0.14	43.14±1.12	5.21±0.01	0.41±0.01	40.32±0.41	1.44±0.01	0.70±0.01

Biochar

Parameters						
Carbon (C), %	Hydrogen (H), %	Nitrogen (N), %	Oxygen (O), %	H/C	O/C	$\frac{O+N}{C}$
75.29±1.17	1.21±0.03	1.70±0.01	21.80±0.55	0.19±0.01	0.35±0.01	0.31±0.02
68.30±1.14	1.36±0.04	1.58±0.01	28.76±0.24	0.23±0.01	0.38±0.01	0.44±0.02
53.64±1.21	0.97±0.01	1.30±0.01	44.09±0.31	0.21±0.01	0.48±0.01	0.84±0.03

(Biochar rows: GSB 600 °C, CSB 600 °C, WSB 600 °C)

carbon content were found to be around 68.91, 8.71, 11.52, and 10.86%, while in wheat straw biomass, 66.12, 9.18, 7.9, and 16.8%, respectively. More volatile matter in selected feedstock justifies that all crop residues are more suitable for biofuel production because of their rapid devolatilization rate during pyrolysis. Similarly, lower moisture content was found in all feedstock, indicating thermal uniformity during the carbonization process. The higher heating value of groundnut shell, chickpea straw, and wheat straw was around 16.23, 15.21, and 14.74 MJ/kg, which was very analogous to other agro residues [19, 20].

The elementary analyses results indicate that all three biomass feedstock, groundnut shell, chickpea straw, and wheat straw, contain a higher percentage of carbon to be around 50.12, 48.10, and 43.14%, with oxygen content to be about 42.80, 42.31, and 40.32%, while less percentage of hydrogen about 5.41, 5.23, and 5.12%, whereas the negligible percentage of nitrogen about 0.6, 0.40, and 0.41% were recorded in groundnut shell, chickpea straw, and wheat straw, respectively. The less percentage of nitrogen and sulfur in selected biomass feedstock results in less emission of SOx, and NOx in the atmosphere. The H:C and O:C ratio for groundnut shell, chickpea straw, and wheat straw was also reported in Table 3.

Mass Yield

It was observed (Supplemental Figure S1) that for all biomass feedstock, maximum biochar yield was recorded for 500 °C, followed by 550 °C, and 600 °C. The biochar yields at 500, 550, and 600 °C were estimated at 35.7, 31.08, and 28.57% for groundnut shells; 33.14, 31.5, and 27% for chickpea straw, and 37.71, 36.28, and 35.25% for wheat straw biomass respectively. The obtained results are well supported by Sun et al. [21]. It was observed that, as pyrolysis temperature increased, the biochar yield diminished, but the produced biochar at higher temperature showed excellent physicochemical composition, surface morphology. Rehrah et al. [22] also reported that the physicochemical composition of the biomass feedstock has a direct impact on the quantity and quality of produced biochar.

It is evident from (Supplemental Figure S1) on increasing the operating temperature; the biochar yield was significantly reduced. In biomass pyrolysis, up to 110–150 °C mass loss was took place due to the evaporation of moisture, while above 150 °C biomass starts breaking down, and because of degradation of cellulose and hemicellulose, it turns down into vapour containing gas mixed organic substances. While lowering the biochar yield at maximum pyrolysis temperature is possibly due to the decomposition of more organic compounds at higher pyrolysis temperature. Ahmad et al. [15] also stated that biochar yield decreased from 37 to 22%

with a temperature rise from 600 to 700 °C due to lignin and cellulose degradation in the raw material.

Characterization of Biochar

Physicochemical properties of biochar are mainly varying considerably with biomass feedstock and operating conditions like pyrolysis temperature, residence time, and heating rate. Biochar characteristics such as larger surface area, micro, and mesoporous structure, highest pH, more carbon and hydrogen content, and greater availability of surface functional groups (O–H and C=C/C=O) can favor maximum Zn adsorption capacity from aqueous solution [23]. Therefore, in the present study, to understand the efficacy of biochar for Zn adsorption, the physicochemical characterization of produced biochar from wheat straw, chickpea straw, and groundnut shell in terms of elementary analysis, surface morphological, and FTIR analysis were carried out and reported as follows:

Elementary Analysis of Biochar

The physicochemical properties of biochar are mainly dependent on biomass feedstock, pyrolysis temperature, and residence time [24]. In the present study, pyrolysis temperature showed a significant influence on biochar yield and its basic composition. Elementary analysis of biochar indicates that all biochar contains maximum availability of total carbon ranging between 53.64 and 75.29% (Table 3). Further, hydrogen, nitrogen, and oxygen content in all biochar samples were in the range of 0.97–1.36, 1.30–1.70, and 21.80–44.09%, respectively. These results are consistent with the previous findings by Sun et al. [21]. The results also revealed that as pyrolysis temperature raised, the available total carbon content also increased, whereas lowering the percentage of hydrogen and oxygen resulted in a reduction in the molar concentration of H/C, O/C, and (O+N)/C. The cation exchange capacity of biochar indicates the negative charge load on its surface, which plays an important role in the adsorption process [25]. More cation exchange capacity in biochar is due to the availability of organic compounds that result in a higher O/C ratio in biochar.

The O/C ratio for GSB, CSB, and WSB at 600 °C were found to be around 0.35, 0.38, and 0.48, respectively, showing that WSB 600 °C have more O/C ratio as compared to other biochars. The H/C ratio of biochar denotes its aromaticity [26]. The GSB, CSB, and WSB 600 °C possess a molar H/C concentrations were 0.19, 0.23, and 0.21, respectively. The obtained results justified that produced biochar samples at a higher pyrolysis temperature of about 600 °C were completely carbonized, referred to as amorphous biochar. whereas the polarity index indicator, the (O+N)/C, was found minimal in all biochars obtained at 600 °C.

Scanning Electron Microscope (SEM) Analysis

The SEM analysis was employed to identify the surface morphology difference between the precursor material and produced biochars. The SEM morphology of groundnut shells, GSB 500, GSB 550, and GSB 600 °C are shown in Fig. 1a–d. From these figures, it was observed that the surface morphology of the groundnut shell was smooth before carbonization. In contrast, the rough and porous structure was observed in biochars after pyrolysis. The pores observed in these biochar structures are typically large micro and mesopores, which act as a passage for adsorbates to the micro-porous system present on the cell walls. As carbonization proceeds and more volatile material is removed, the GSB 600 °C shows a better pore structure than GSB 500 and GSB 550 °C. The pore volume of groundnut shell biochar was found to increase from 0.027 to 0.17 cm³/g with an increase in pyrolysis temperature. According to Thommes et al. [27], the surface morphology of biochar suggests micro and mesoporous structures. Similar morphology was also reported by Ahmad et al. [28], Nascimento et al. [29], and Possa et al. [30] for groundnut shell, wood sawdust, and sewage sludge biochar samples.

The obtained results from Fig. 2a–d, indicate the surface structure of chickpea straw biochars, which was mainly affected by pyrolysis temperature. For chickpea straw, a non-porous fibrous morphology was observed. It is a sponge-like layered surface for all biochars with interconnected channels processed at different temperatures. The porous structure was developed during pyrolysis due to the degradation of cellulose and hemicellulose. In addition, the decomposition of lignin at elevated temperature, which enables the carbon composition to burn off, resulted in a more porous texture. The pore volume of chickpea straw biochar was recorded between 0.017 and 0.10 cm³/g, indicating its mesoporous structure. A mesoporous structure for chickpea straw derived biochar was also observed in previous literature as reported by Nazari et al. and Tasim et al. [31, 32], respectively.

From Fig. 3a–d, it is observed that the surface morphology of wheat straw was found to be an irregular structure with a smooth surface, whereas it was found to be porous and rough morphology with different diameters for all obtained biochars. As pyrolysis temperature increased from 500 to 600 sᵒC, the pore volume was also found subsequently improved from 0.04 to 0.21 cm³/g indicating meso and microporous structure of biochars. Interestingly, biochar derived at 600 °C showed a micro-porous honeycomb-like morphology, and lots of nanoholes were found on its surface.

SEM analysis revealed that all biochars had a uniform porous structure with a wide availability of pores than raw material. The micro and mesoporous structure of biochars produced at higher pyrolysis temperature show more sorption sites and strong pore filling affinity for Zn adsorption

Fig. 1 SEM images of **a** groundnut shell, **b** GSB 500 °C, **c** GSB 550 °C, and **d** GSB 600 °C
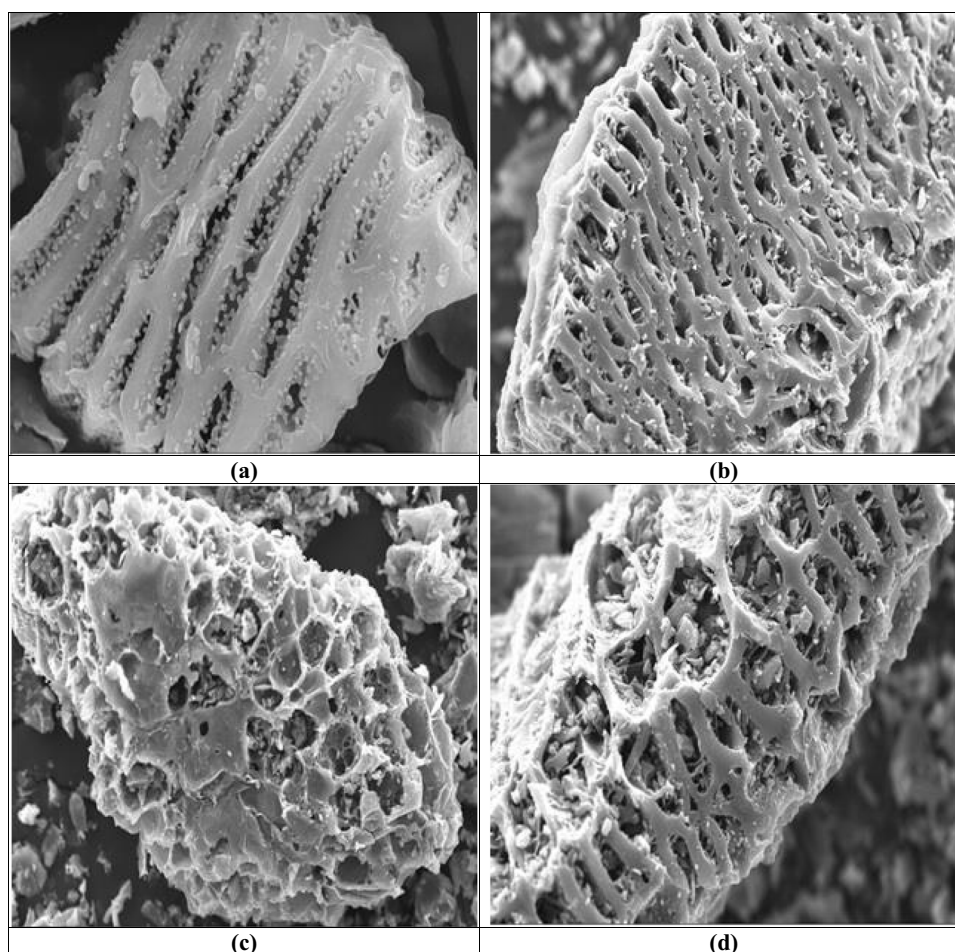
[33]. Additionally, the micro and mesoporous structure of biochar facilitate the transformation of Zn between the pores and results in an increase in adsorption capacity [34]. As compared to other biochar materials, wheat straw-derived biochar showed a good surface morphology in terms of its microporous structure, the honeycomb-like structure obtained at a pyrolysis temperature of 600 °C.

Fourier Transforms Infrared Spectroscopy (FTIR) Analysis

FTIR spectra of groundnut shell and its biochar samples obtained at 500, 550, and 600 °C are shown in Fig. 4.

From Fig. 4, it was evident that a broad peak between 3000 and 3300 cm^{-1} is occurred because of C-H stretching vibrations of lignocellulosic components present in groundnut shell biomass [35]. These peaks were slightly reduced in obtained biochars as pyrolysis temperature increased, justifying the degradation of structural components of the groundnut shell feedstock [36]. $C = O$ and $C = C$ double bond stretching vibrations could be allocated to the peak at the $1750 - 1570$ cm^{-1} band in the feedstock and produced biochar [37]. Groundnut shell has a strong peak at about 2331 cm^{-1} which corresponds to

strong $C = C$ stretching vibrations [38]. The –COO– bond stretched carboxylate vibration was directly linked to a prominent band at 1070 cm^{-1} [39]. At 1750–1570 cm^{-1}, GSB 600 °C displayed greater bond stretching vibrations than GSB 500 and 550 °C. Based on the above results, it was concluded that obtained biochar samples at higher pyrolysis temperature showed a more carbonaceous structure with an extremely cross-linked channel matrix.

Similarly, for chickpea straw biomass and biochars, as shown in (Supplemental Figure S2), a broad peak of about 3300 and 3400 cm^{-1} for feedstock was due to the asymmetric distension of the O–H bonds by the water derivatives. C–O stretching vibrations for all samples were observed at a band spectrum of about 1000 cm^{-1}. In the 1440 cm^{-1} area, the wavelength indicates the bending vibration of the C–H groups of alkanes [31]. While for biochar samples, peaks observed at 1500 and 1600 cm^{-1} were attributed to vibrations of $C = C$ aromatic ring bending, which also appeared for spectra between 756 and 586 cm^{-1} by a narrower band [40]. The wavelength observed in all biochar specimens at 1559 cm^{1} confirmed the stretching and tensile motions of the functional group amines ($-$NH).

Fig. 2 SEM images of **a** chickpea straw, **b** CSB 500 °C, **c** CSB 550 °C, and **d** CSB 600 °C
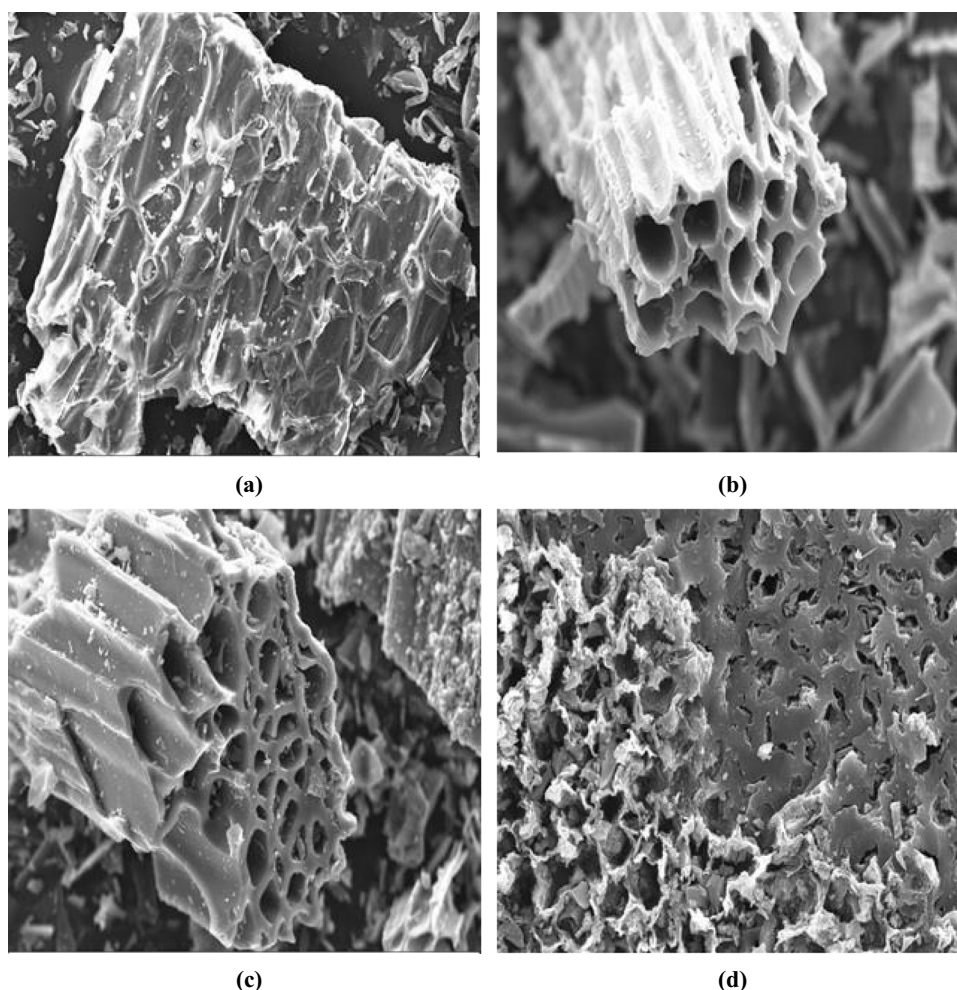

(a)

(b)

(c)

(d)

Figure 5 shows the availability of functional groups for different wavelengths of wheat straw biomass and its biochars. The bands around 3500 and 3300 cm^{-1} and among 1650 and 1600 cm^{-1} were directly linked to −OH stretching and water distortion. The peaks were assigned as the –CH stretched at 3026 cm^{-1}, as well as the peaks were detected as the C–O stretching of monosaccharides at 1260 to 1000 cm^{-1} [41]. In WSB 500, 550, and 600 °C, aliphatic CH$_2$ stretching from cellulose, hemicellulose, or lignin and fatty acids available in the biomass were assigned to bands at 1435 and 2948 cm^{-1} [42]. In carboxylic and ester groups, certain bands reflect extends due to C=O (1790 cm^{-1}), C=C, and C=O in aromatic rings (1560 cm^{-1}), COOH, and CHO at 1435 cm^{-1} [43, 44].

Based on the FTIR spectra of all selected biomass and its obtained biochar samples, it was observed that a peak obtained at 2920 cm^{-1} for all biomass samples showed asymmetric and non-symmetric C–H stretching vibrations of aliphatic acids. However, as pyrolysis temperature increased from 500 to 600 °C of the peak was slightly disappeared, justifying the development of the aromatic structure of

biochar, which was compatible with Zn adsorption. A condensed aromatic structure was occurred in high temperature biochars mainly due to the complete thermal cracking of cells, hemicelluloses, lignin, and proteins available in biomass at higher pyrolysis temperature. Additionally, available functional groups on biochar surface obtained at higher pyrolysis temperature of 600 °C such as carboxylic acid, amines, phenol, and some alcohol based functional groups that play a remarkable role in Zn adsorption or cation and anion sorption capacity of biochar. Also, biochar produced at higher pyrolysis temperature showed the presence of carbonyl, carboxylate, hydroxyl, and phenolic groups, which may improve the specific metal binding capacity.

Screening of Biochar for Removal of Zn

Based on the above results, superior biochar was selected according to its physicochemical composition, morphology, and availability of functional groups for the adsorption or removal of Zn. Among the different temperatures like 500, 550, and 600 °C, biochar produced at 600 °C from all the three

Fig. 3 SEM images of **a** wheat straw, **b** WSB 500 °C, **c** WSB 550 °C, and **d** WSB 600 °C
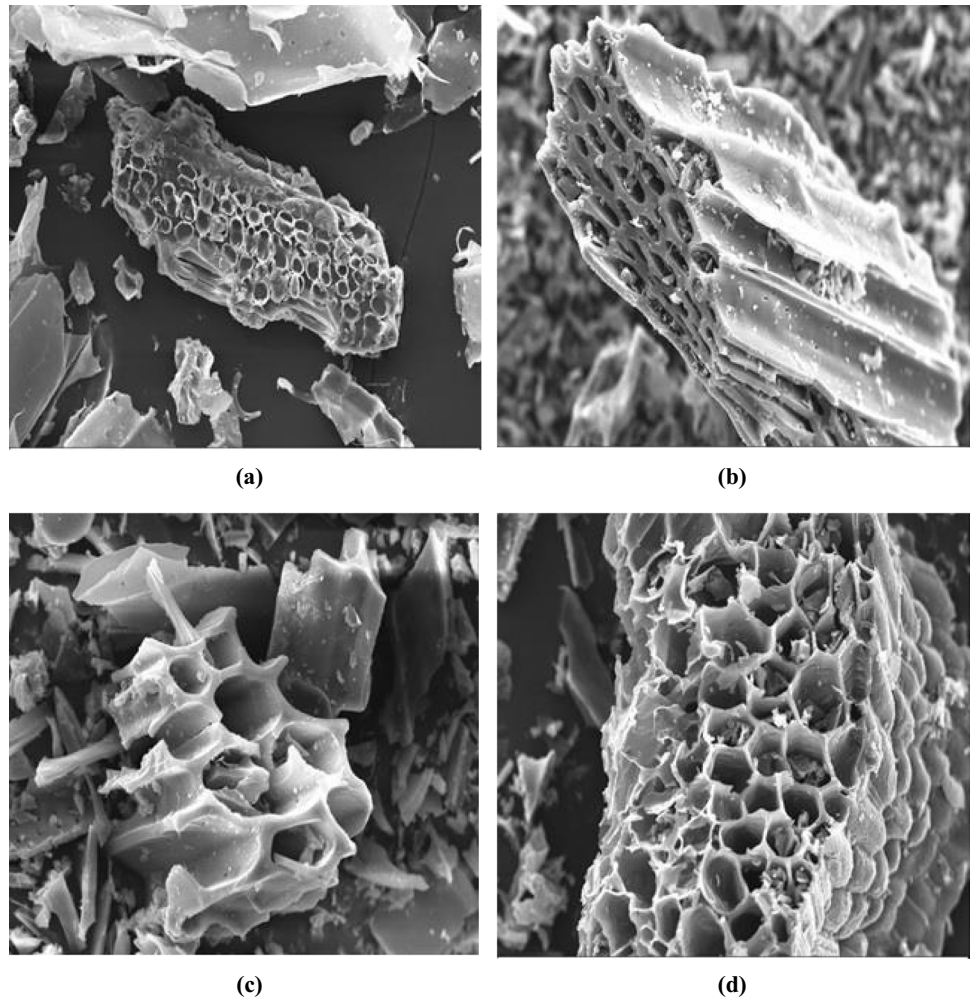

(a)

(b)

(c)

(d)

Fig. 4 FTIR spectra of groundnut shell and its biochar produced at different temperatures
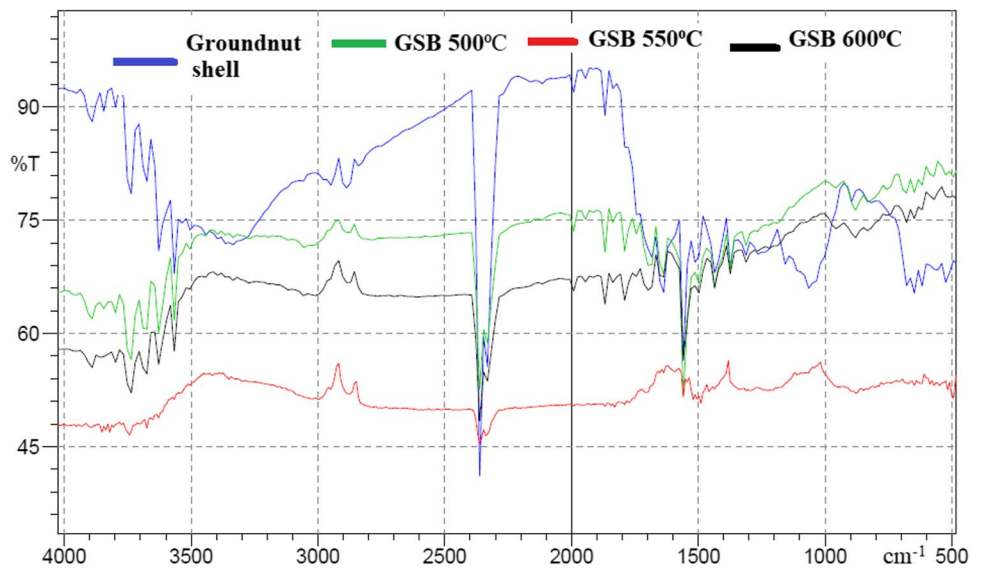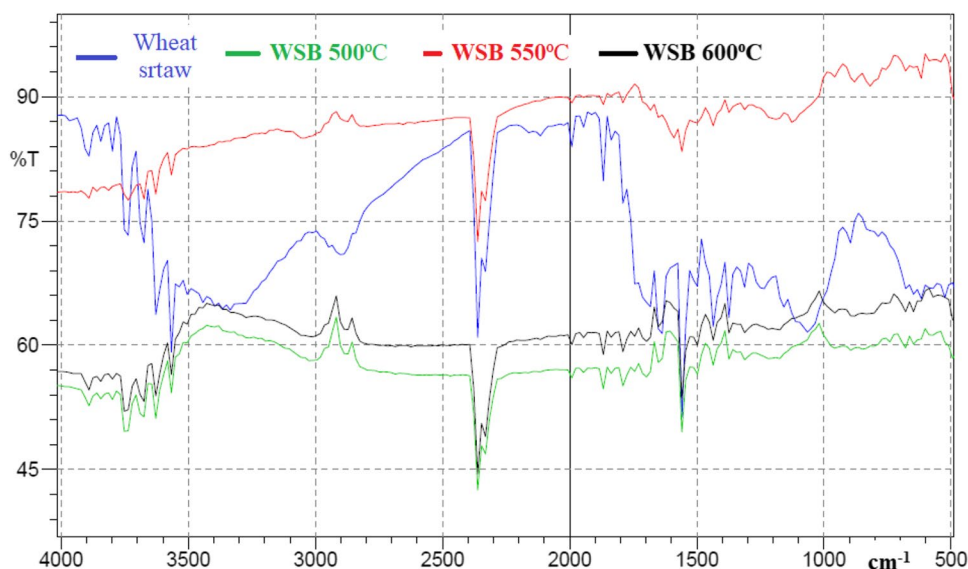
Fig. 5 FTIR spectra of wheat straw and its biochar produced at different temperature

feedstock showed well-developed porous structure and wide availability of functional groups; therefore, maximum temperature condition of 600 °C was considered more appropriate for the adsorption process. The initial screening of 40 ppm Zn solution on GSB, CSB, and WSB produced at 600 °C was studied. The experimental layout for the selection of biochar is listed in (Supplemental Table S1). A solution consisting of 40 ppm Zn and 2 gm of GSB, CSB, and WSB was incubated for 240 min at ambient temperature. Among all selected biochars, WSB prepared at 600 °C demonstrated 78% removal of Zn (Supplemental Table S1). Therefore, all the remaining optimization investigations are thus carried out using wheat straw biochar produced at 600 °C.

Optimization of Process Parameters for the Removal of Zn

To achieve optimum removal performance, it is necessary to optimize the process parameters such as biochar dosage, heavy metal concentration, and contact time for the removal of Zn from an aqueous solution. Taking three variables, three level Box-Behnken experimental designs combined with the design of the experiment, the acceptable configuration of ideal conditions for maximum removal of Zn by wheat straw derived biochar was established. As per Box-Behnken design, 15 experiments were performed as listed in Table 2 for obtaining the percent reduction in Zn as responses for each test as shown in (Supplemental Table S2).

Regression Models and the Effect of Parameters on the Removal of Zn

The method of Zn adsorption from the aqueous solution was based on the dosage of biochar, the concentration of heavy

metal, and the contact period. Therefore, using the response surface technique, these process parameters were optimized. A polynomial function of the second-order [Eq. (2)] was equipped with the observational data provided in (Supplemental Table S2). Equation (3) indicates the expected percent removal of Zn, percent as a component of biochar dosage (A), the concentration of heavy metals (B), and treatment time (C) represented in the coded form.

The quadratic model was adapted to acquire the observational results, whereas the statistical significance of Zn was calculated as shown in Table 4. The R^2 value was calculated and observed to be 0.999 for Zn by the least square method, indicating a good fit of the model to the results. For Zn, the model F value of 799.23 is indicating that the design was acceptable ($P < 0.01$). There was an important linear term (A, B, and C) for Zn ($P < 0.01$). The lack of fit F value was not significant, which suggested that the model built was adequate for the approach to be expected. Furthermore, with an optimized R^2 of 0.998 for Zn, the expected R^2 of 0.995 was the suitable standard. It is indicated that the words of non-significance are not included in the model. This model could therefore be used to traverse the design area.

The findings of the variance analysis (ANOVA) demonstrated that the linear and quadratic terms of the biochar dosage, concentration of heavy metals, and contact time for Zn extraction were relevant at the 1% stage. Although the biochar dosage and heavy metal concentration interaction effects and the biochar dosage and contact time were also significant at the 1% level, the heavy metal concentration and contact time interaction were extremely considerable at the 5% level. The comparable impact of each factor on the removal efficiency of Zn is determined by the F values of the ANOVA functions as listed in Table 4. The higher F values indicated that biochar dose ($F = 3221.84$) was the

Table 4 Analysis of variance for percentage removal of Zn

Source	Sum of squares	df	Mean sum of squares	F value
Model	5595.60	9	621.73	799.23**
A	2506.32	1	2506.32	3221.84**
B	1902.52	1	1902.52	2445.67**
C	149.56	1	149.56	192.26**
AB	606.88	1	606.88	780.14**
AC	39.38	1	39.38	50.62**
BC	5.20	1	5.20	6.68*
A^2	94.35	1	94.35	121.29**
B^2	167.11	1	167.11	214.82**
C^2	181.57	1	181.57	233.41**
Residual	3.89	5	0.78	
Lack of fit	1.28	3	0.43	0.33 ns
Pure error	2.61	2	1.31	
Cor total	5599.49	14		
R^2	0.9993			
Adj R^2	0.9981			
Pred R^2	0.9953			
Std. dev	0.88			
Mean	70.18			
C.V. %	1.26			

Table 5 Optimization criteria for different process variables and responses for removal of Zn

Parameter	Goal	Lower limit	Upper limit
Biochar dose, (gm)	Range	1	3
Heavy metal concentration, (ppm)	Range	20	60
Contact time, (min)	Range	120	360
Removal of Zn, (%)	Maximize	26.38	96.85

would be within the economic context for the maximum percent reduction of Zn [45]. Table 5 shows the optimization criteria for different process variables and responses for the removal of Zn. To optimize the process parameters for the percentage removal of Zn by optimization algorithms, which finds a point that maximizes the desirability function, all three control parameters (biochar dose (A), the concentration of heavy metals (B), and the contact period (C) and first response (percent removal of Zn) were given equal importance of '3.' At a random reference point, the target setting progresses and continues up the highest slope on the response interface for Zn's highest percentage withdrawal level.

The optimum conditions thus obtained for biochar dosage, the concentration of heavy metals, and the contact period were 2.90 gm, 22 ppm, and 309 min correspondingly. The percentage removal value for Zn was recorded to be around 97.16%, referring to those values for processing parameters. One of the important aims of the current research is to verify the result of optimized process parameters based on RSM. Biochar doses of 3 g/L, heavy metal concentrations of 22 ppm), and contact times of 310 min were used for the individual run. Within a variance of 2% that confirmed the design, the percentage removal Zn obtained was reasonable.

most influencing parameter followed by heavy metal concentration ($F = 2445.67$) and contact time ($F = 192.26$). The regression calculation showing the effect of process parameter on percent removal of Zn in real terms of biochar dose (A), heavy metal concentration (B), and contact time (C) can be given by following Eq. (4)

$$Y_{Zn} = 179.395 - 33.43A - 3.2331B - 0.231C + 0.6158AB + 0.0261AC$$
$$- 0.0047BC + 5.055A^2 + 0.0168B^2 + 0.0048C^2 \quad (4)$$

In the present study, the sign and the magnitude of the coefficient mainly describe the significance of the consequence of the variables. Negative linear terms indicated a decrease in the reduction of Zn, but the presence of positive interaction terms between the biochar dosage and the concentration of heavy metals, the biochar dosage, and the time of contact of the process suggested that a rise in their levels also increased the reduction of Zn [Eq. (4)]. The positive values of quadratic terms of biochar dosage, the concentration of heavy metals, and the contact period indicated that higher values of these parameters increased the removal of Zn.

Numerical Optimization of Process Variables

The parameters were defined in such a way that the independent features, such as the biochar dose (A), the concentration of heavy metals (B), and the contact period (C),

Three-Dimensional Response Surface Plots

Response surface plots represent three-dimensional descriptions of the reactions, which provide a straightforward assessment of the impact of the two or more variables. Three-dimensional surface plots (Fig. 6a–c) were developed for the fitted model as a function of two variables to represent the collective effect of two parameters on the reduction of Zn, whereas the third variable, was at its central value. A point in these graphs can evaluate the ideal values of variable factors.

Impact of the Biochar Dose The adsorbent dose is one of the significant parameters which affect the adsorption process [46]. This is an essential factor since it determines
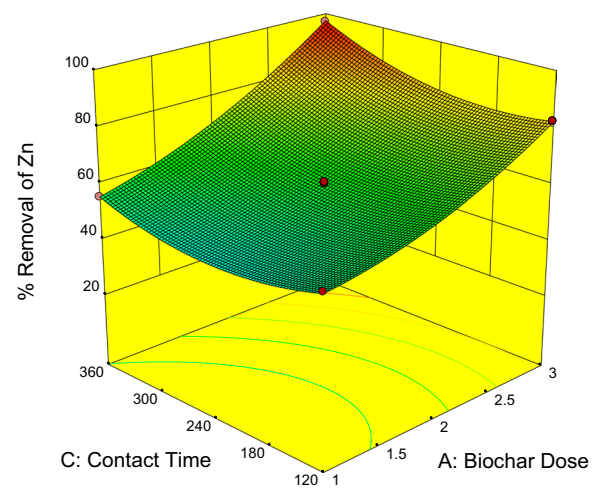
Fig. 6 Three-dimensional surface plots of the combined effect of the **a** biochar dose and heavy metal concentration, **b** heavy metal concentration and contact time, and **c** biochar dose and contact time on Zn removal
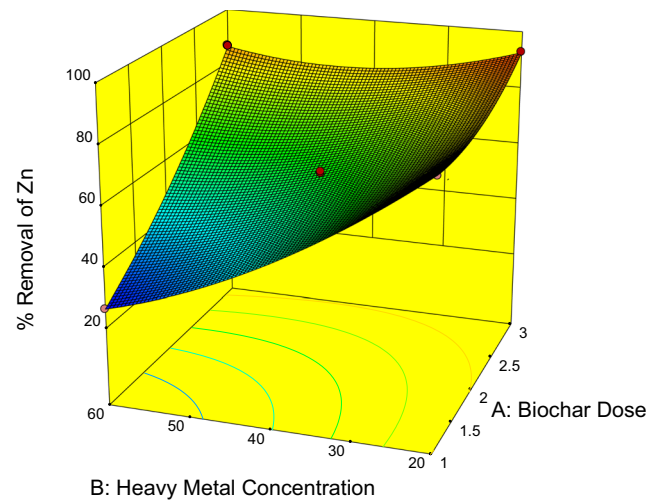
(a)
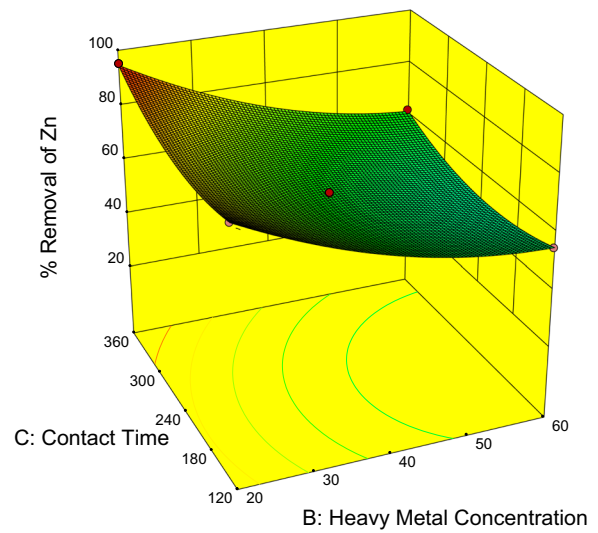
(b)

(c)

the potential of an adsorbent for a known input adsorbate concentration [47]. The experimental results with different adsorbent doses are listed in (Supplemental Table S2). The plot (Fig. 6a) for a combined effect of biochar dose and heavy metal concentration at constant contact time (240 min) shows that at any fixed contact time, the removal percentage increases with increasing biochar dose. The extraction percentage was reported, gradually increasing from 26 to 97% for Zn with a dosage increase between 1 and 3 g/L. The improvement in the adsorbent dose causes an increase in the extraction of Zn percent. The reported pattern is attributed to increased accessibility of binding sites with higher dose levels. However, as the binding sites were depleted, the extraction of Zn was decreased or stayed unchanged (Fig. 6a). Similar findings were reported by Tsai and Chen [48], where the authors revealed that the majority of adsorption sites were increased by the rise in adsorbent dosage (i.e., 0.10–0.30 g/L).

Influence of Heavy Metal Ions Figure 6b shows the combined effect of heavy metal concentration and contact time on the uptake of Zn by WSB. Percent removal was plotted as a function of heavy metal concentration to analyze the influence of the initial Zn concentration from 20 to 60 ppm. As a rise in heavy metal concentration up to a crucial point of 21 ppm, it was elevated and then either balanced off or reduced. This may be due to the accumulation of the biochar's metal binding sites, and the rate balanced at a 20–23 ppm heavy metal content. A similar trend agrees with Liu and Zhang [49]. It was investigated that the contact time for 95% removal equilibrium was less than 5 h in the concentration range of 10–20 ppm for pinewood and rice husk derived biochar.

Influence of Contact Period As a function of contact time, the percentage elimination of Zn was assessed. With an increase in contact time (1–3 h), the Zn elimination rate was found to be increased from 26 to 97% (Fig. 6c). Moreover, primarily due to the greater surface area of the adsorbent being available at the time, the rate was significantly greater. After a contact time of 4 h, the saturation rate for Zn removal was reached. A similar result was also reported by Pellera et al. [50]. The initially rapid rate of adsorption within the first few minutes of interaction was followed by a relatively slow one before the equilibrium state was achieved, according to Pellera et al. [50]. This was due to the presence of abundant vacated active biochar sites, although these active sites were progressively saturated over time during adsorption. The time required to achieve balance, on the other hand, was roughly 2–4 h, with no

noticeable effect as the contact time increased by up to 24 h. Nazari et al. [31] stated that high specific surface area and pore volumes encourage metal transformation between biochar pores and ultimately increase metal adsorption, and this process occurred in the present investigation for wheat straw derived biochar.

Conclusion

The present study investigated the physicochemical characterization of biochar derived from wheat straw, chickpea straw, and groundnut shell, where the effectiveness of wheat straw biochar was assessed for Zn adsorption from an aqueous solution. Wheat straw biochar produced at higher pyrolysis temperature (600 °C) showed the highest Zn removal efficiency from aqueous solution might be due to its salient features such as microporous structure, carbon content, oxygen to carbon ratio, and greater availability of surface functional groups. Zinc adsorption is significantly influenced by all three investigational parameters namely biochar dosage, heavy metal concentration, and contact period. The obtained findings concluded that wheat straw biochar has great potential for zinc removal from an aqueous solution. whereas biochar derived from groundnut shells and chickpea straw can be used for the soil remediation.

Authors' Contributions Divyesh R. Vaghela carried out experimental work and wrote draft, Ashish Pawar was reviewed, and edited manuscript. Deepak sharma was examined and editd the manuscript.

Data Availability Not applicable to this work.

Declarations

Ethics Approval This work does not involve experiments using humans or other animals.

Consent to Participate Approved.

Consent to Publish Approved.

Competing Interests. The authors declare that they have no competing interests.

References

1. Singh, R, Bisaria, K, Chugh, P, Batra, L, Sinha, S (2021) Agricultural waste: a potential solution to combat heavy metal toxicity. In: Gothandam, KM, Srinivasan, R, Ranjan, S, Dasgupta, N, Lichtfouse, E (ed) Environmental Biotechnology. Environmental Chemistry for a Sustainable World. Springer, Cham, pp 101–124. https://doi.org/10.1007/978-3-030-77795-1_4

2. Jaishankar M, Tseten T, Anbalagan N et al (2014) Toxicity, mechanism and health effects of some heavy metals. Interdiscip Toxicol 7:60–72. https://doi.org/10.2478/intox-2014-0009

3. Schwarzenbach RP, Egli T, Hofstetter TB et al (2010) Global Water Pollution and Human Health. Annu Rev Environ Resour 35:109–136. https://doi.org/10.1146/annurev-environ-100809-125342

4. Elwakeel KZ, Elgarahy AM, Khan ZA et al (2020) Perspectives regarding metal/mineral-incorporating materials for water purification: with special focus on Cr removal. Mater Adv 1:1546–1574. https://doi.org/10.1039/D0MA00153H

5. Panwar NL, Pawar A, Salvi BL (2019) Comprehensive review on production and utilization of biochar. SN Appl Sci 1:168. https://doi.org/10.1007/s42452-019-0172-6

6. Zhou Y, Qin S, Verma S et al (2021) Production and beneficial impact of biochar for environmental application: a comprehensive review. Bioresour Technol 337:125451. https://doi.org/10.1016/j.biortech.2021.125451

7. Hiloidhari M, Das D, Baruah DC (2014) Bioenergy potential from crop residue biomass in India. Renew Sustain Energy Rev 32:504–512. https://doi.org/10.1016/j.rser.2014.01.025

8. Mishra A, Kumar A, Ghosh S (2018) Energy assessment of second generation (2G) ethanol production from wheat straw in Indian scenario. Biotech 8:142. https://doi.org/10.1007/s13205-018-1135-0

9. Augustine MA, Singh VCJ, Sekhar SJ (2021) Spent tea waste as a biomass for co-gasification enhances the performance of semi-industrial gasifier working on groundnut shell. Biomass Bioenergy 145:105964. https://doi.org/10.1016/j.biombioe.2021.105964

10. Maurya O, Kumar H (2018) Growth of chickpea production in India. J pharmacogn phytoch 7:1175–1177

11. Ahmad M, Rajapaksha AU, Lim JE et al (2014) Biochar as a sorbent for contaminant management in soil and water: A review. Chemosphere 99:19–33. https://doi.org/10.1016/j.chemosphere.2013.10.071

12. Gonzaga MIS, Mackowiak CL, Comerford NB et al (2017) Pyrolysis methods impact biosolids-derived biochar composition, maize growth and nutrition. Soil Tillage Res 165:59–65. https://doi.org/10.1016/j.still.2016.07.009

13. Frišták V, Friesl-Hanl W, Wawra A et al (2015) Effect of biochar artificial ageing on Cd and Cu sorption characteristics. J Geochem Explor 159:178–184. https://doi.org/10.1016/j.gexplo.2015.09.006

14. Tak B, Tak B, Kim Y et al (2015) Optimization of color and COD removal from livestock wastewater by electrocoagulation process: application of Box-Behnken design (BBD). J Ind Eng Chem 28:307–315. https://doi.org/10.1016/j.jiec.2015.03.008

15. Ahmad M, Lee SS, Dou X et al (2012) Effects of pyrolysis temperature on soybean stover- and peanut shell-derived biochar properties and TCE adsorption in water. Bioresour Technol 118:536–544. https://doi.org/10.1016/j.biortech.2012.05.042

16. Kim W-K, Shim T, Kim Y-S et al (2013) Characterization of cadmium removal from aqueous solution by biochar produced from a giant Miscanthus at different pyrolytic temperatures. Bioresour Technol 138:266–270. https://doi.org/10.1016/j.biortech.2013.03.186

17. Jindo K, Mizumoto H, Sawada Y et al (2014) Physical and chemical characterization of biochars derived from different agricultural residues. Biogeosciences 11:6613–6621. https://doi.org/10.5194/bg-11-6613-2014

18. Vyas D, Sayyad F, Khardiwar M, Kumar S (2015) Physico-chemical Properties of Briquettes from Different Feed Stock. Curr World Environ. 10:263–269. https://doi.org/10.12944/CWE.10.1.32

19. Leng S, Li W, Han C et al (2020) Aqueous phase recirculation during hydrothermal carbonization of microalgae and soybean straw: a comparison study. Bioresour Technol 298:122502. https://doi.org/10.1016/j.biortech.2019.122502

20. Galhano dos Santos R, Bordado JC, Mateus MM (2018) Estimation of HHV of lignocellulosic biomass towards hierarchical cluster analysis by Euclidean's distance method. Fuel 221:72–77. https://doi.org/10.1016/j.fuel.2018.02.092

21. Sun J, Lian F, Liu Z et al (2014) Biochars derived from various crop straws: Characterization and Cd(II) removal potential. Ecotoxicol Environ Saf 106:226–231. https://doi.org/10.1016/j.ecoenv.2014.04.042

22. Rehrah D, Reddy MR, Novak JM et al (2014) Production and characterization of biochars from agricultural by-products for use in soil quality enhancement. J Anal Appl Pyrolysis 108:301–309. https://doi.org/10.1016/j.jaap.2014.03.008

23. Zhao M, Dai Y, Zhang M et al (2020) Mechanisms of Pb and/or Zn adsorption by different biochars: Biochar characteristics, stability, and binding energies. Sci Total Environ 717:136894. https://doi.org/10.1016/j.scitotenv.2020.136894

24. Panwar NL, Pawar A (2022) Influence of activation conditions on the physicochemical properties of activated biochar: a review. Biomass Convers Biorefin 12:925–947. https://doi.org/10.1007/s13399-020-00870-3

25. Lee JW, Kidder M, Evans BR et al (2010) Characterization of Biochars Produced from Cornstovers for Soil Amendment. Environ Sci Technol 44:7970–7974. https://doi.org/10.1021/es101337x

26. Uchimiya M, Wartelle LH, Lima IM, Klasson KT (2010) Sorption of Deisopropylatrazine on Broiler Litter Biochars. J Agric Food Chem 58:12350–12356. https://doi.org/10.1021/jf102152q

27. Thommes M, Kaneko K, Neimark AV et al (2015) Physisorption of gases, with special reference to the evaluation of surface area and pore size distribution (IUPAC Technical Report). Pure Appl Chem 87:1051–1069. https://doi.org/10.1515/pac-2014-1117

28. Ahmad M, Lee SS, Oh S-E et al (2013) Modeling adsorption kinetics of trichloroethylene onto biochars derived from soybean stover and peanut shell wastes. Environ Sci Pollut Res 20:8364–8373. https://doi.org/10.1007/s11356-013-1676-z

29. Nascimento PFP, Sousa JF, Oliveira JA et al (2017) Wood sawdust and sewage sludge pyrolysis chars for CO_2 adsorption using a magnetic suspension balance. Can J Chem Eng 95:2148–2155. https://doi.org/10.1002/cjce.22861

30. Possa RD, Sousa JF, Oliveira JA et al (2018) Dynamic adsorption of H_2S in a fixed bed of sewage sludge pyrolysis char. Braz J Pet Gas 12:77–90. https://doi.org/10.5419/bjpg2018-0008

31. Nazari S, Rahimi G, Khademi Jolgeh Nezhad A (2019) Effectiveness of native and citric acid-enriched biochar of Chickpea straw in Cd and Pb sorption in an acidic soil. J Environ Chem Eng 7:103064. https://doi.org/10.1016/j.jece.2019.103064

32. Tasim B, Masood T, Shah ZA et al (2019) Quality Evaluation of Biochar Prepared from Different Agricultural Residues. SJA 35:134–143. https://doi.org/10.17582/journal.sja/2019/35.1.134.143

33. Zhang P, Sun H, Ren C et al (2018) Sorption mechanisms of neonicotinoids on biochars and the impact of deashing treatments on biochar structure and neonicotinoids sorption. Environ Pollut 234:812–820. https://doi.org/10.1016/j.envpol.2017.12.013

34. Jiang B, Lin Y, Mbog JC (2018) Biochar derived from swine manure digestate and applied on the removals of heavy metals and antibiotics. Bioresour Technol 270:603–611. https://doi.org/10.1016/j.biortech.2018.08.022

35. Bhaduri D, Saha A, Desai D, Meena HN (2016) Restoration of carbon and microbial activity in salt-induced soil by application of peanut shell biochar during short-term incubation study. Chemosphere 148:86–98. https://doi.org/10.1016/j.chemosphere.2015.12.130

36. Mimmo T, Panzacchi P, Baratieri M et al (2014) Effect of pyrolysis temperature on miscanthus (Miscanthus × giganteus) biochar physical, chemical and functional properties. Biomass Bioenergy 62:149–157. https://doi.org/10.1016/j.biombioe.2014.01.004

37. Miller GP, Kintigh J, Kim E et al (2008) hydrogenation of single-wall carbon nanotubes using polyamine reagents: combined experimental and theoretical study. J Am Chem Soc 130:2296–2303. https://doi.org/10.1021/ja0775366

38. Chu G, Zhao J, Chen F et al (2017) Physi-chemical and sorption properties of biochars prepared from peanut shell using thermal pyrolysis and microwave irradiation. Environ Pollut 227:372–379. https://doi.org/10.1016/j.envpol.2017.04.067

39. Ghaffar A, Ghosh S, Li F et al (2015) Effect of biochar aging on surface characteristics and adsorption behavior of dialkyl phthalates. Environ Pollut 206:502–509. https://doi.org/10.1016/j.envpol.2015.08.001

40. Özsin G, Kılıç M, Apaydın-Varol E, Pütün AE (2019) Chemically activated carbon production from agricultural waste of chickpea and its application for heavy metal adsorption: equilibrium, kinetic, and thermodynamic studies. Appl Water Sci 9:56. https://doi.org/10.1007/s13201-019-0942-8

41. Qayyum MF, Steffens D, Reisenauer HP, Schubert S (2012) kinetics of carbon mineralization of biochars compared with wheat straw in three soils. J Environ Qual 41:1210–1220. https://doi.org/10.2134/jeq2011.0058

42. Mohanty P, Nanda S, Pant KK et al (2013) Evaluation of the physiochemical development of biochars obtained from pyrolysis of wheat straw, timothy grass and pinewood: Effects of heating rate. J Anal Appl Pyrolysis 104:485–493. https://doi.org/10.1016/j.jaap.2013.05.022

43. Peterson SC, Jackson MA (2014) Simplifying pyrolysis: Using gasification to produce corn stover and wheat straw biochar for sorptive and horticultural media. Ind Crops Prod 53:228–235. https://doi.org/10.1016/j.indcrop.2013.12.028

44. Song Y, Wang F, Bian Y et al (2012) Bioavailability assessment of hexachlorobenzene in soil as affected by wheat straw biochar. J Hazard Mater 217–218:391–397. https://doi.org/10.1016/j.jhazmat.2012.03.055

45. Rahman N, Nasir M (2018) Application of Box-Behnken design and desirability function in the optimization of Cd(II) removal from aqueous solution using poly(o-phenylenediamine) / hydrous zirconium oxide composite: equilibrium modeling, kinetic and thermodynamic studies. Environ Sci Pollut Res 25:26114–26134. https://doi.org/10.1007/s11356-018-2566-1

46. El-Ashtoukhy E-SZ, Amin NK, Abdelwahab O (2008) Removal of lead (II) and copper (II) from aqueous solution using pomegranate peel as a new adsorbent. Desalination 223:162–173. https://doi.org/10.1016/j.desal.2007.01.206

47. Aydın H, Bulut Y, Yerlikaya Ç (2008) Removal of copper (II) from aqueous solution by adsorption onto low-cost adsorbents. J Environ Manage 87:37–45. https://doi.org/10.1016/j.jenvman.2007.01.005

48. Tsai W-T, Chen H-R (2013) Adsorption kinetics of herbicide paraquat in aqueous solution onto a low-cost adsorbent, swine-manure-derived biochar. Int J Environ Sci Technol 10:1349–1356. https://doi.org/10.1007/s13762-012-0174-z

49. Liu Z, Zhang F-S (2009) Removal of lead from water using biochars prepared from hydrothermal liquefaction of biomass. J Hazard Mater 167:933–939. https://doi.org/10.1016/j.jhazmat.2009.01.085

50. Pellera F-M, Giannis A, Kalderis D et al (2012) Adsorption of Cu(II) ions from aqueous solutions on biochars prepared from agricultural by-products. J Environ Manage 96:35–42. https://doi.org/10.1016/j.jenvman.2011.10.010